American Journal of Energy and Power Engineering
2017; 4(5): 25-31
http://www.aascit.org/journal/ajepe
ISSN: 2375-3897

AASCIT American Association for Science and Technology

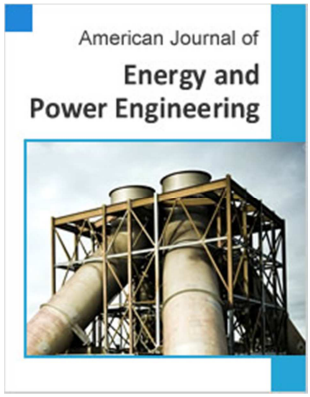

Keywords
Coupled Reactor,
Chemical Looping Combustion,
Numerical Simulation

Received: June 19, 2017
Accepted: September 19, 2017
Published: October 17, 2017

Coupled Reactor Chemical Looping Behavior Combustion Simulation

Namory Camara[1], Lu Huilin[2]

[1]Department of Physics, Faculty of Science and Techniques, Bamako, Mali
[2]School of Energy Science and Engineering, Harbin Institute of Technology, Harbin, China

Email address
namorymcamara@yahoo.fr (N. Camara)

Citation
Namory Camara, Lu Huilin. Coupled Reactor Chemical Looping Behavior Combustion Simulation. *American Journal of Energy and Power Engineering.* Vol. 4, No. 5, 2017, pp. 25-31.

Abstract
Based on the particle kinetic and chemical kinetics theory, chemical looping combustion calculation model to simulate the inner coupling reactor chemical looping combustion process, access to the inside of the reactor flow field characteristics and distribution of the various components, and good to capture the atmosphere of the reactor particles exhibit a non-uniform flow structure nucleus. The simulation results also given temperature distribution as well as the export of particle mass flow rate and concentration of each component in the reactor over time for design optimization coupled reactor provides a certain basis.

1. Introduction

Chemical looping combustion is an effective way to capture carbon dioxide, which is coupled by the air from the reactor and the reactor fuel in the fuel reactor, a gas fuel reacts with the metal oxide, the metal oxide in oxygen reduction out and the formed metal is reduced by the air delivered to the carrier in the reactor, then the reactor with the incoming oxygen in the air oxidation reaction, and then, the resulting metal oxide is recycled into the fuel type reactor react with the fuel. The oxygen-carrying metal oxide oxygen transfer agent, to avoid direct contact with oxygen and fuel, and thus achieve a good capture of carbon dioxide [1]. In this process, CO_2 is not produced N_2 dilution, while separation of CO_2 without any energy, in addition, since the fuel conversion process and no direct contact with the air, thus eliminating the NOx fundamentally produce [2], this approach to develop new ways of recycling CO_2. Alberto et al [3] for the different oxygen carriers and range of operating conditions of the fuel system has been studied, pointed out the low oxygen carrying capacity of the circulation rate is relatively large, the other sequestered by oxygen loading and circulation rate is also affected by the reaction rate impact. Jin et al [4]. For the reaction of the fuel reactor were 3D simulation, and pointed out that reducing the particle size and the operating speed can be increased fuel conversion rate, the bed bubble enhance mixing, while reducing the rate of reaction. Mattisson et al [5] pointed out that the use of plug flow model can not accurately predict the interaction sequestered inside the reactor, the application of fluid dynamics model can better reflect the gas-solid between. Iggland et al. [6] studied the coupling reactor gasification process, and noted that the particle size has little impact on fuel conversion, particle size distribution after cleavage by fluidized impact is small. Mahalatkar [7] to fuel a research reactor, and were compared with experimental, research shows that two-fluid model combined with particle kinetic theory may well capture the bubbles appear in the bed area of high concentration in the fuel, which can cause the reaction rate is reduced, the fuel difficult to burn completely. Based on the particle

kinetic and chemical kinetics theory, a solid flow-model coupling reaction of the coupler flow combustion process is simulated.

2. Mathematical Model

2.1. Flow Model

Gas phase and solid phase continuity equation is:

$$\frac{\partial}{\partial t}(\varepsilon_g \rho_g) + \nabla \cdot (\varepsilon_g \rho_g \boldsymbol{u}_g) = S_{gs} \tag{1}$$

$$\frac{\partial}{\partial t}(\varepsilon_s \rho_s) + \nabla \cdot (\varepsilon_s \rho_s \boldsymbol{u}_s) = S_{sg} \tag{2}$$

Where, S_{gs} and S_{sg} are quality gas and solid phase per unit time unit volume generated, and:

$$S_{gs} = -S_{sg} \tag{3}$$

Gas phase and solid phase of each quality increment equal to the quality of their components and the increment.

$$S_{gs} = \sum_{i=1}^{N_g} S_{g,i} \text{ and } S_{sg} = \sum_{i=1}^{N_s} S_{s,i} \tag{4}$$

Wherein, $S_{g,i}$ and $S_{s,i}$, respectively, to generate a gas phase and a solid phase with in the volume of the amount of the i-th component unit time per unit. Multi-component gas mixture consisting of may be assumed as an ideal gas, density determined from the ideal gas equation of state.

$$\frac{1}{\rho_g} = \frac{RT}{p} \sum_{i=1}^{N_g} \frac{Y_{g,i}}{M_{g,i}} \tag{5}$$

Wherein, R, T, P, respectively, is the universal gas constant, temperature and pressure; $Y_{g,i}$ and $M_{g,i}$ is the mass fraction of gas components and molar mass.

Gas and solid phase momentum conservation equation is:

$$\frac{\partial}{\partial t}(\varepsilon_g \rho_g \boldsymbol{u}_g) + \nabla \cdot (\varepsilon_g \rho_g \boldsymbol{u}_g \boldsymbol{u}_g) = \varepsilon_g \nabla \cdot \boldsymbol{\tau}_g + \varepsilon_g \rho_g \boldsymbol{g} - \varepsilon_g \nabla \boldsymbol{p} - \beta(\boldsymbol{u}_g - \boldsymbol{u}_s) + S_{gs} \boldsymbol{u}_g \tag{6}$$

$$\frac{\partial}{\partial t}(\varepsilon_s \rho_s \boldsymbol{u}_s) + \nabla \cdot (\varepsilon_s \rho_s \boldsymbol{u}_s \boldsymbol{u}_s) = \varepsilon_s \nabla \cdot \boldsymbol{\tau}_s + \varepsilon_s \rho_s \boldsymbol{g} - \varepsilon_s \nabla \boldsymbol{p} + \beta(\boldsymbol{u}_g - \boldsymbol{u}_s) + S_{sg} \boldsymbol{u}_s \tag{7}$$

The gaseous components conservation equation:

$$\frac{\partial}{\partial t}(\rho_g Y_{g,i}) + \nabla \cdot (\rho_g Y_{g,i} \boldsymbol{u}_g) = -\nabla \cdot J_{g,i} + S_{g,i} \tag{8}$$

Where, i = 1 ~ N_g , $Y_{g,i}$, $J_{g,i}$ components were local mass fraction and diffusion flux i, and the diffusion flux can be calculated according to Fick's law

$$J_{g,i} = -(\rho_g D_i + \frac{\mu_t}{\sigma_Y}) \nabla \cdot Y_{g,i} \tag{9}$$

In the formula, D_i is the molecular diffusion coefficient of component i; σ_Y represents Schmidt number, take 0.7.

Solid phase components conservation equation:

$$\frac{\partial}{\partial t}(\rho_s Y_{s,i}) + \nabla \cdot (\rho_s Y_{s,i} \boldsymbol{u}_s) = S_{s,i} \tag{10}$$

Wherein, $Y_{s,i}$ for the local mass fraction of component i, i = 1 ~ N_s .

Gas and energy conservation equations for the solid phase:

$$\frac{\partial}{\partial t}(\alpha_g \rho_g c_g T_g) + \nabla \cdot (\alpha_g \rho_g c_g T_g \boldsymbol{u}_g) = \nabla(\lambda_g \nabla T_g) + \varphi_{gs}(T_g - T_s) + \sum S_{gi} c_g T_g \tag{11}$$

$$\frac{\partial}{\partial t}(\alpha_s \rho_s c_s T_s) + \nabla \cdot (\alpha_s \rho_s c_s T_s \boldsymbol{u}_s) = \nabla(\lambda_s \nabla T_s) + \varphi_{sg}(T_s - T_g) + \sum S_{si} c_{si} T_s \tag{12}$$

Wherein c, λ, φ denote the specific heat capacity, thermal conductivity and heat transfer coefficient and white.

$$c_g = \sum Y_i c_{gi} \qquad c_s = \sum Y_i c_{si} \tag{13}$$

$$\lambda_g = \sum_i \frac{Y_i \lambda_{gi}}{\sum_{i \neq j} Y_i \Phi_{ij}} \qquad \lambda_s = \sum_i Y_{si} \lambda_{si} \tag{14}$$

$$\lambda_{gi} = \mu_g \left(c_{gi} + \frac{5}{4} \frac{R}{M_{gi}} \right) \quad , \quad \lambda_{si} = \mu_s \left(c_{si} + \frac{5}{4} \frac{R}{M_{gi}} \right) \quad , \quad \Phi_{ij} = \frac{1 + \sqrt{\frac{\mu_i}{\mu_j} (\frac{M_i}{M_j})^{0.25}}}{\sqrt{8(1 + \frac{M_i}{M_j})}} \tag{15}$$

$$\varphi_{sg} = \varphi_{gs} = \frac{6 \lambda_g \varepsilon_g \varepsilon_s Nu_s}{d_s^2} \tag{16}$$

$$Nu_s = \left(7 - 10\alpha_g + 5\alpha_g^2\right)\left(1 + 0.7\,\mathrm{Re}_s^{0.2}\,\mathrm{Pr}^{1/3}\right) + \left(1.33 - 2.4\alpha_g + 1.2\alpha_g^2\right)\mathrm{Re}_s^{0.7}\,\mathrm{Pr}^{1/3} \tag{17}$$

2.2. Chemical Reaction Model

In this study, the gas phase include CH_4, CO_2, H_2O, O_2 and N_2 five components, including NiO and Ni particle phase two components, in order to simplify the calculation model assumes NiO and Ni particle size and apparent density the same heat transfer coefficient. Air reactors and reactor fuel chemical reaction equations are as follows:

$$2Ni + O_2 \rightarrow 2NiO \qquad \Delta H = -479.4 kJ / mol\ O_2 \tag{18}$$

$$CH_4 + 4NiO \rightarrow 4Ni + CO_2 + 2H_2O \qquad \Delta H = 156.5 kJ / mol\ CH_4 \tag{19}$$

In selecting a chemical reaction model, using a condensing nuclear reaction model [8, 9]:

$$r_1 = k_1 S_1 \varepsilon_g \frac{\rho_g x_{O_2}}{M_{O_2}} \qquad S_1 = \frac{6}{d_s} \varepsilon_s \qquad k_1 = 0.8677 \exp\left(-\frac{43390}{RT}\right) \tag{20}$$

$$r_2 = k_2 S_2 \varepsilon_g \frac{\rho_g x_{CH_4}}{M_{CH_4}} \qquad S_2 = \frac{6}{d_s} \varepsilon_s x_{O_2} \qquad k_2 = 0.0327 \exp\left(-\frac{8854.1}{RT}\right) \tag{21}$$

3. The Initial and Boundary Conditions

Calculation model in accordance with [10] constructed an experimental model, shown in Figure 1. Four partial separation, fuel reactors and the composition of the bench overflow device by the air in the reactor, the reactor bottom air inlet air evenly; the bottom of the reactor fuel inlet to the fuel gas uniformly, top to pressure outlet, the outlet pressure of 1atm; bottom overflow means uniform gas inlet. For the physical parameters of the model in [11] to select, see Table 1.

Table 1. *Simulation parameters.*

Symbol	Physical meaning	Analog values	Unit
ρ_s	Particle density	3446	kg/m^3
D	Particle diameter	200	μm
$H_1/ H_2 / H_3$	Air reactors, reactor fuel and return feeder height	1.9/0.15/0.5	m
$D_1/ D_2 / D_3$	Air reactors, reactor fuel and return feeder diameter	0.19/0.14/0.19	m
$v_1/ v_2 / v_3$	Air reactors, reactor fuel and return feeder inlet gas velocity	2 /0.07/0.12	m/s
T	The initial temperature	1123	K
$\alpha_{s,,}$	The initial particle packing density	0.5	--
Y_{s0}	The initial mass fraction of particulate phase components	Ni(0.422), NiO(0.578)	--
$H_{1,0}/ H_{2,0}/ H_{3,0}$	Air reactors, reactor fuel and return feeder initial bed height	0.35/0.15/0.15	m
e	Particles elastic recovery coefficient	0.9	--
e_w	Wall of restitution elasticity coefficient	0.9	--
Y_{ar}	Reactor inlet air mass fraction of gas component	O_2(0.23), N_2(0.77)	--
Y_{fr}	A fuel gas inlet of the reactor mass fraction	CH_4(0.9), N_2(0.1)	--

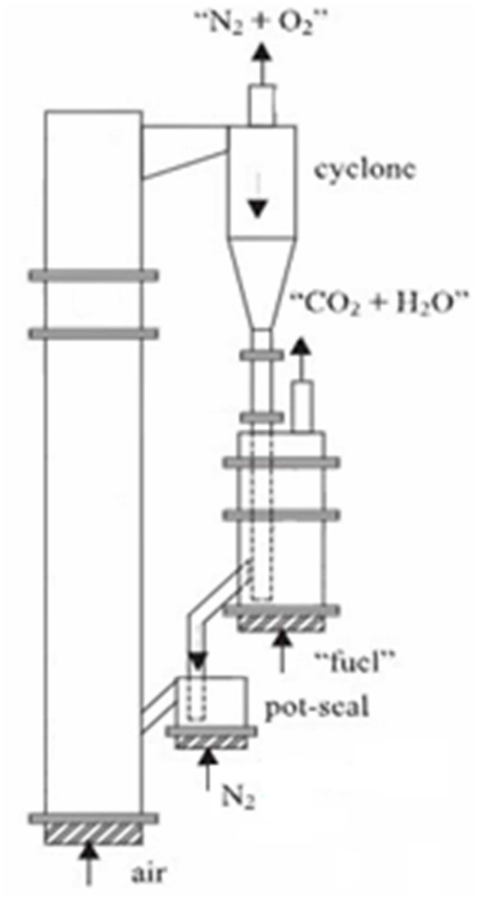

Figure 1. *Schematic diagram of the fluidized-bed gasification bed.*

4. Simulations and Analysis

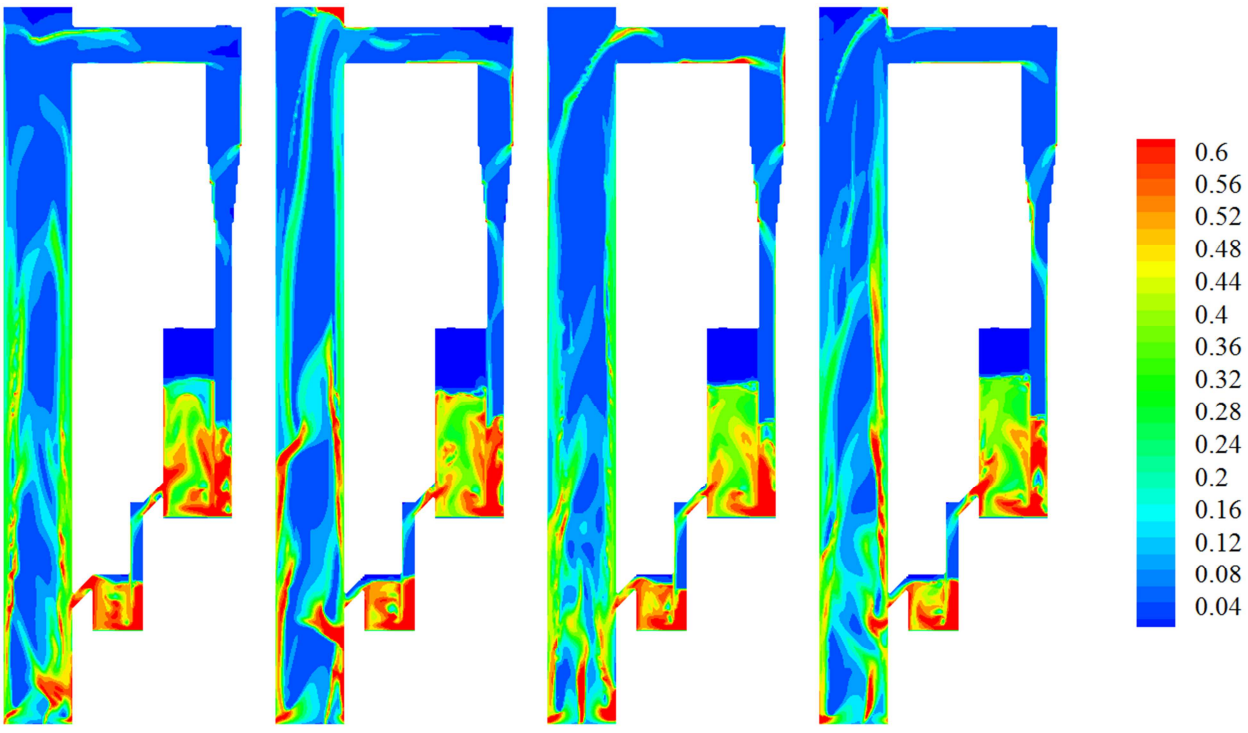

Figure 2. *Instantaneous particle concentration distribution phase.*

Figure 2 shows the distribution of the coupling reactor instantaneous particle concentration, can be seen from the figure, the air at the bottom of the reactor a higher concentration, and the concentration decrease with increasing height, the central region of the particles flow upward, while the wall particulate poly group appear, and some particles are gas into the separator under gravity into the fuel reactor, the fuel equivalent of bubbling bed reactor, generating bubbles at the entrance, as the bubbles rise to the surface rupture, particles along the wall downward movement. Particles from the reactor portion of the fuel will flow into the overflow device, and then returned to the air through the overflow means in the reactor, which completed the cycle.

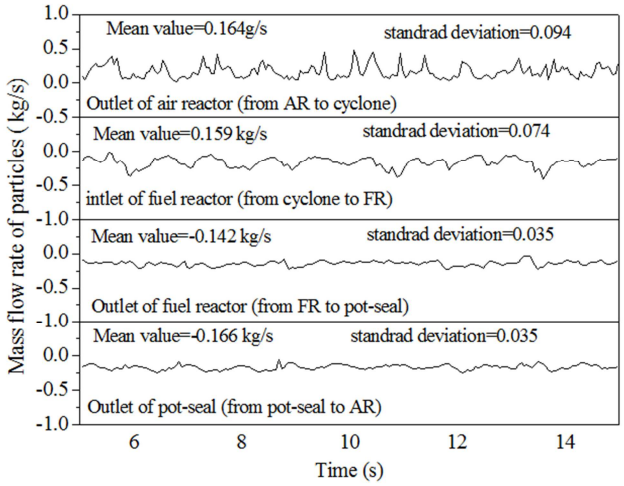

Figure 3. *Different particle flow rate Position instantaneous distribution.*

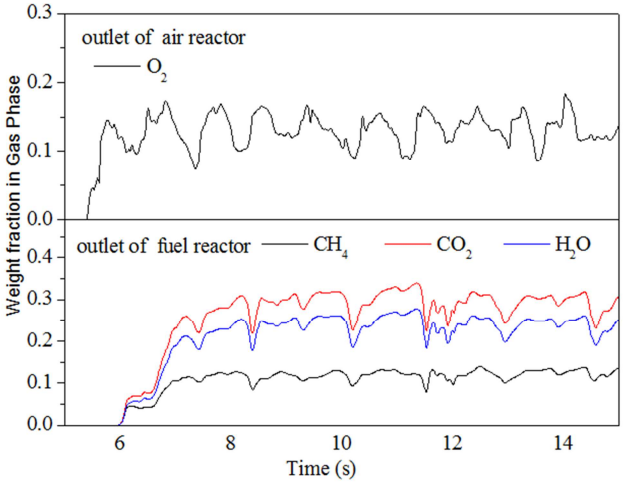

Figure 4. *Reactor outlet instantaneous species mass fraction distribution.*

Figure 3 is coupled reactor located in different locations instantaneous particle flow rate distribution, it can be seen from the figure the mass flow rate of particles is oscillating, the figure also shows the standard differential particle flow rate, wherein the air outlet of the reactor standard deviation of the largest particle flow rate, which shows that export the most intense particle mass flow oscillation, which may be due to the high velocity air in the reactor, pulsating strong, while non-uniform particles dispersed particles agglomerate and coexistence of the bed flow structure at the outlet of the particle flow rate is also presented strong reasons for instability.

Figure 4 is a mass fraction of each component of the reactor with the fuel air outlet of the reactor over time. As can be seen from the figure, the fuel in the reactor and an air bubble disturbance reactor multiscale presence of non-uniform flow structure over time so that the components exhibit strong oscillations. 5s fuel when the fuel from the inlet into the bottom of the reactor, as the reaction proceeds, the continuous generation of carbon dioxide and water vapor, the mass fraction also increases, approximately at 8s, reactor fuel mass fraction of each component tends to a more stable state, the methane content is about 0.12 changes, and Water vapor and carbon dioxide mass fraction of about 0.24 and 0.29 in change. Compared with the fuel of the reactor, the reactor since the air speed is high, so that unreacted oxygen reaches the reactor outlet in the first reactor in the fuel gas, as the reaction proceeds, the oxygen mass fraction is also stabilized but due to the particles agglomerate and the mass flow rate of pulsation, the mass fraction of oxygen also around 0.12 in the oscillation.

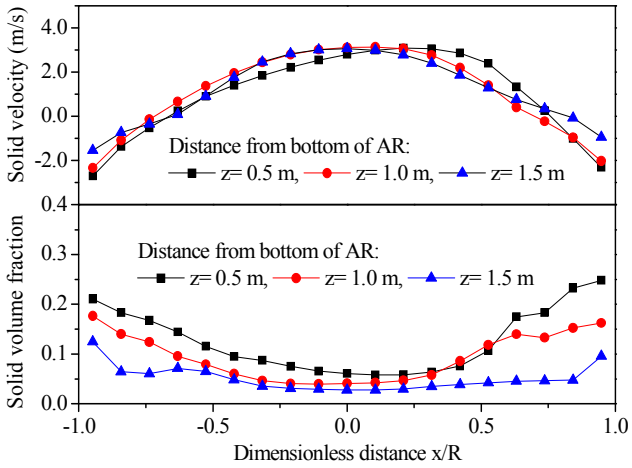

Figure 5. *Air reactor concentration and average Velocity distribution of the particles radially.*

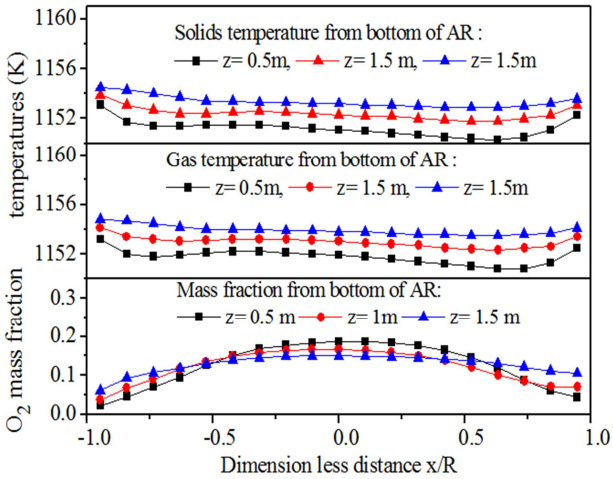

Figure 6. *Air reactor, O_2 mass fraction and vapor solidus temperature distribution in the radial direction.*

Figure 5 is a different height in both the atmosphere of the reactor when the particle concentration and average velocity distribution in the radial direction. It can be seen from the figure, the particles exhibit a low concentration of the central region, along the wall surface is gradually increased, the largest concentration of non-uniform distribution in the vicinity of the wall surface of the trend, and as the height increases, the concentration decreases, binding velocity profile, the center at the maximum speed is positive, indicating that the upward movement of the particles are, and wall particles is negative, the particles move downward, the whole atmosphere of the reactor showing concentrated on the thick side walls under a lean too thin intermediate nucleus flow structure.

Figure 6 is a different height in the atmosphere of the reactor radially O_2 content distribution, O_2 content rendered radially center high distribution trend lower side wall, which is related to the distribution of particle concentration, particle concentration due to the larger wall surfaces. Therefore, the amount of oxygen consumption increases. As the altitude increases, O_2 content decreased, while the figure shows the temperature distribution along the radial gas-solid, gas-solid phase distribution trends are basically the same, namely the center of the lower temperature than the wall, because the wall concentration high, the reaction rate is high, and the reaction is exothermic, and therefore relatively high wall temperature from the numerical point of view, gas temperature should be slightly higher than the solidus temperature.

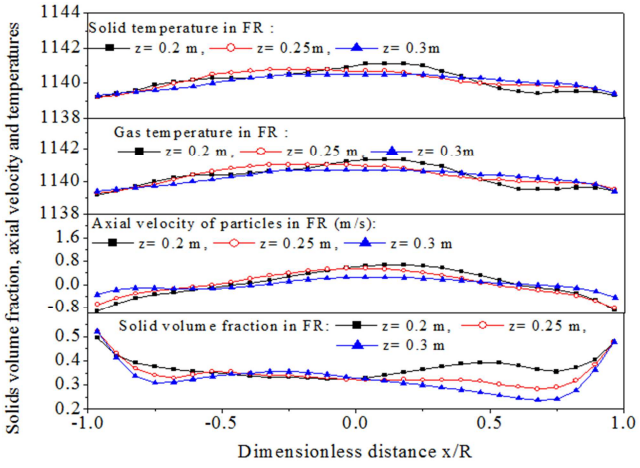

Figure 7. *Average particle concentration, velocity Gas solidus temperature along the radial distribution of the fuel in the reactor.*

Figure 7 is within the average particle concentration of the reactor fuel velocity and temperature of gas-solid phase distributed radially at different heights. As can be seen from the figure, the particle concentration along the bed of the radial center of the low-side wall exhibits high distribution trend, the low center particle concentration is caused due to the presence of bubbles, and the central region the particle velocity is positive, showing upward movement of the particles wall surface area particle velocity is negative, the particles fall, to form particles in the bed of the macro-cycle sport. From the temperature profile can be seen in the bed temperature profile exhibits a low wall at the center of the high-side non-uniform trend, as the height increases, the radial temperature distribution difference decreases, gas and solid phase temperature distribution trend is consistent in the numerical difference is small.

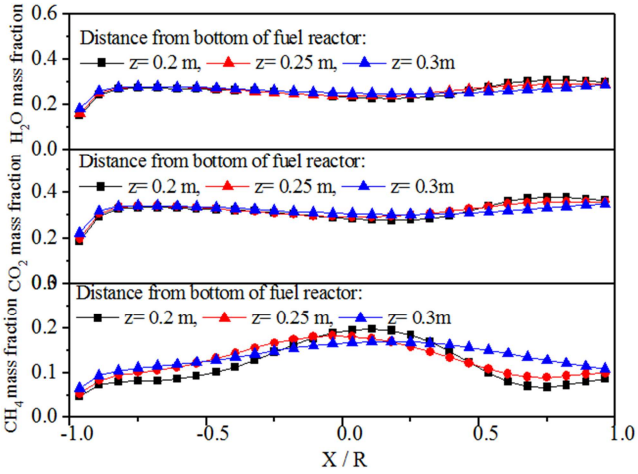

Figure 8. *Reactor fuel CO_2, H_2O and CH_4 mass fraction of the radial distribution.*

Figure 8 shows a fuel reactor CH_4, CO_2 and H_2O mass fraction distribution trends in the radial direction. As can be seen from the figure, the central region of high methane content, and the wall surface is low, mainly due to the presence of the central region of the bubble caused by gas mainly in the form of bubbles through the bed material, as well as a high degree of increase in the reaction, CH_4 content decreased, while the share of quality corresponding increase of CO_2 and H_2O. CO_2 and H_2O content decreased to the left, this position may be caused by the overflow port.

5. Conclusion

Particle kinetic and chemical reaction kinetics theory, the coupling reactor gas-solid flow reactor model, the numerical simulation of coupled chemical looping combustion reactor process, access to the features and components of the distribution of the flow field based on the reaction. Simulation results show that the air in the reactor particles exhibit dilute concentrated on the lower side wall intermediate concentrated nucleus lean flow structure, and reactor fuel particles in the bed is also showing a structure similar to circulate within the bubbling bed. The study also found that for the reactor outlet, the flow rate of the particles and the mass fraction of each component there are different degrees of oscillation, the oscillation is most obvious with O_2, which is operating with the air in the reactor as well as non-uniform flow structure of the entire reactor conditions.

References

[1] Anders Lyngfelt, Bo Leckner, Tobias Mattisson. A fluidized-bed combustion process with inherent CO_2 separation; application of chemical-looping combustion [J]. Chemical Engineering Science, 2001, 56: 3101-3113.

[2] Ishida, M., Jin, H. A novel chemical-looping combustor without NOx formation [J]. Industrial and Engineering Chemistry Research, 1996, 35: 2469-2472.

[3] Alberto Abad, Juan Adánez, Francisco García-Labiano, Luis F. de Diego, PilarGayán, Javier Celaya. Mapping of the range of operational conditions for Cu-, Fe-, and Ni-based oxygen carriers in chemical-looping combustion [J]. Chemical Engineering Science, 2007, 62: 533-549.

[4] Xiaojia Wang, Baosheng Jin, Wenqi Zhong, Yong Zhang, Min Song. Three-dimensional simulation of a coal gas fueled chemical looping combustion process [J]. International Journal of Greenhouse Gas Control, 2011, 5: 1498-1506.

[5] Tobias Mattisson, ErikJerndal, Carl Linderholm, Anders Lyngfelt, Reactivity of a spray-dried $NiO/NiAl_2O_4$ oxygen carrierfor chemical-looping combustion [J]. Chemical Engineering Science, 2011, 66: 4636-4644.

[6] Martin Iggland, Henrik Leion, Tobias Mattisson, Anders Lyngfelt. Effect of fuel particle size on reaction rate in chemical looping combustion [J]. Chemical Engineering Science, 2010, 65: 5841-5851.

[7] Kartikeya Mahalatkar, John Kuhlman, E. David Huckaby Thomas O'Brien, Computational fluid dynamic simulations of chemical looping fuel reactors utilizing gaseous fuels [J], Chemical Engineering Science, 2011, 66: 469-479.

[8] Jonghwun Jung, Isaac K. Gamwo. Multiphase CFD-based models for chemical looping combustion process: Fuel reactor modeling [J], Powder Technology, 2008, 183: 401-409.

[9] H. Kruggel-Emden, F. Stepanek, A. Munjiza. A comparative study of reaction models applied for chemical looping combustion [J]. Chemical Engineering Research and Design, 2011, 89: 2714-2727.

[10] E. Johansson, A. Lyngfelt, T. Mattisson, F. Johnsson Gas leakage measurements in a cold model of an interconnected fluidized bed for chemical-looping combustion [J], Powder Technology, 2003, 134: 210-217.

[11] Philipp Kolbitsch, Tobias Proll, Hermann Hofbauer. Modeling of a 120kW chemical looping combustion reactor system using a Ni-based oxygen carrier [J]. Chemical Engineering Science, 2009, 64: 99-108.